Modulational instability in nonlinear saturable media with competing nonlocal nonlinearity

Conrad Bertrand Tabi, Hippolyte Tagwo, and Timoléon Crépin Kofané

Phys. Rev. E **106**, 054201 — Published 4 November 2022

DOI: 10.1103/PhysRevE.106.054201

Modulational instability in nonlinear saturable media with competing nonlocal nonlinearity

Conrad Bertrand Tabi*
Department of Physics and Astronomy, Botswana International University of Science and Technology, Private Mail Bag 16 Palapye, Botswana

Hippolyte Tagwo†
Laboratory of Mechanics, Department of Physics, Faculty of Science, University of Yaoundé I, P.O. Box 812, Yaoundé, Cameroon

Timoléon Crépin Kofané‡
Department of Physics and Astronomy, Botswana International University of Science and Technology, Private Mail Bag 16 Palapye, Botswana
Laboratory of Mechanics, Department of Physics, Faculty of Science, University of Yaoundé I, P.O. Box 812, Yaoundé, Cameroon and
Centre d'Excellence Africain en Technologies de l'Information et de la Communication, University of Yaoundé I, Cameroon

(Dated: October 10, 2022)

The modulational instability (MI) phenomenon is addressed in a nonlocal medium under controllable saturation. The linear stability analysis of a plane wave solution is used to derive an expression for the growth rate of MI that is exploited to parametrically discuss the possibility for the plane wave to disintegrate into nonlinear localized light patterns. The influence of the nonlocal parameter, the saturation coefficient, and the saturation index are mainly explored in the context of a Gaussian nonlocal response. It is pointed out that the instability spectrum, which tends to be quenched by the high nonlocality parameter, gets amplified under the right choices of the saturation parameters, especially the saturation index. Via direct numerical simulations, confirmations of analytical predictions are given, where competing nonlocal and saturable nonlinearities enable the emergence of trains of patterns as manifestations of MI. The comprehensive parametric analysis carried out throughout the numerical experiment reveals the robustness of the obtained rogue waves (RWs), of A- and B-types Akhmediev breathers, as the nonlinear signature of MI, providing the saturation index as a suitable tool to manipulate nonlinear waves in nonlocal media.

I. INTRODUCTION

Generation and propagation of nonlinear structures have been an active research direction for the last few decades. A relevant mathematical model that has been extensively used for many physical realizations in optics [1], Bose-Einstein condensates (BECs) [2], and physics of Langmuir waves in plasmas [3] is the nonlinear Schrödinger (NLS) equation with the self-attractive nonlinearity and its extension, due to the enhancement of nonlinear absorption and nonlinear refractive index [4, 5]. In fact, with the emergence of composite optical materials aiming at photonic applications, the nonlinear optical properties of the constitutive colloidal systems of particles can be controlled, allowing nonlinearity to be managed. Specifically, a suitable choice of nanoparticle volume fraction can allow nullifying the cubic nonlinearity and promote the effects from higher-order nonlinearities [6], including competing nonlinearities. In the latter context, the global nonlinearity results from a few different physical processes, as in BECs with concomitant local and long-range interactions [7] and nematic liquid crystals under competitive thermal and orientational thermal nonlinearities [8]. In other contexts, nonlinearity can be controlled via an adapted nonlocal function of the incident field, commonly known as *nonlocal nonlinearity*.

Contrary to media with conventional nonlinearities, the nonlinear response of nonlocal media depends on the spatial variability of the material's refractive index, i.e., determined by the intensity of the incident field in a certain neighborhood of a given location [9]. Such properties which come with stabilizing features for solitons, can suppress instability [10–12], and support the emergence of new soliton states [13–16]. For instance, nonlocality appears to be an inherent property of thermal media [17, 18], nematic liquid crystals [19], atomic vapors [20], and BECs [21], etc. The nonlocal nonlinearity also exists in liquid infiltrated photonic crystal fibers [22], which supports the existence of nonlocal gap soliton [23]. Another very general important class of nonlocal materials is materials with quadratic nonlinearity [24], from which it was shown that the nonlocal nature of the quadratic nonlinearity could give rise to soliton pulse compression [25], the exotic X waves [26] and can analytically provide the limits of the achievable pulse length [27]. On the same note, it was recently shown that nonlocal Kerr nonlinearity and electromagnetically induced transparency effect might couple and cooperatively support Rydberg-Rydberg interaction between atoms for high-dimensional, nonlocal, and nonlin-

*Electronic address: tabic@biust.ac.bw
†Electronic address: htagwo@gmail.com
‡Electronic address: tckofane@yahoo.com

ear optical X waves to emerge, with manageable characteristics such as low propagation loss, ultraslow propagation velocity, and ultralow generation power [28].

Albeit these advanced and sophisticated theoretical investigations, questions related to competing nonlinear effects, due to their important role in creating stable multidimensional solitons, remain debated. For example, combinations of self-focusing cubic and, particularly, self-defocusing quintic have been frequently reported in optical settings such as liquid waveguides [29–31], special kinds of glasses [29, 32, 33], ferroelectric films [34], and colloidal suspensions of metallic nanoparticles [35, 36], where the colloids offer remarkable flexibility, making it possible to adjust parameters of the cubic-quintic (CQ) nonlinearity (the signs and magnitudes of both the cubic and quintic terms) through the selection of the diameter of the nanoparticles and the filling factor of the suspension. The realization of the CQ nonlinearity was also theoretically elaborated in terms of the Gross-Pitaevskii equation [37] for BECs, where the quintic term accounts for three-body collisions, provided that inelastic effects may be neglected [38–41]. In this context, the adjustment of the nonlinearity may be provided by the Feshbach resonance, which affects the sign and strength of the cubic term [42]. For competing nonlinearities involving saturable nonlinearities, a combination of Kerr nonlinearity and a saturable n-photon resonance was shown to support bistable-soliton pulse propagation [43]. In general, for low field intensities, the saturable nonlinearities depict the usual Kerr response. However, for very intense fields, the dependence of the refraction index on the field intensity saturates. Let us recall that the investigation of saturable nonlinearity, which has been commonly described by two-level atom or exponential models, has been proposed by Maradudin [44]. Any real material has an upper limit to the refractive-index change that can be induced optically. The field strength at which saturation occurs depends on the particular physical processes that cause the nonlinear refractive-index change. In particular, contributions bringing together nonlocal and saturable nonlinearities are still in their infancy. Such a combination implies a nonlinear change of the properties of the medium by the wave itself in a context of very intense fields that cause the refraction index to saturate with increasing field intensity. It is well-known that the evolution of optical materials and laser systems are related. For example, the propagation of picosecond optical pulse in standard silica fibers is governed by the well-known cubic (Kerr effect) NLS equation that includes the group velocity dispersion (GVD) and self-phase modulation (SPM) [45, 46]. In other words, the nonlinear property we are principally concerned with is the field dependence of the refractive index. Moreover, with the advent of robust femtosecond laser systems, nonlinear optical methods such as the optical Kerr effect technique has been extensively used to clarify the nonlinear properties of many organic and inorganic solvents, namely, in a polydiacetylene film, the vibrational dephasing in dimethylsulfoxide and the relaxation of optical Kerr effect in CS_2 and nitrobenzene [47, 48]. Interestingly, as one increases the intensity of the incident light power to produce shorter (femtosecond) pulses, additional nonlinear effects come into play, changing the physical features and the stability of optical soliton propagation essentially, and the dynamics of pulses needs to be described in the frame of a generalized NLS equation that includes higher-order nonlinear terms [49–52] such as Kerr and non-Kerr nonlinearities. Based on particular cases, the saturable nonlinearity can take several forms. In a more generalized formulation, the nonlinear refractive index that describes the nonlinearity saturation is characterized by three independent parameters, mainly the saturation intensity (I_{sat}), the maximum change in the refractive index (n_∞), and the Kerr coefficient (n_2) which appears for small intensities. It is given by the phenomenological expression [53]

$$\Delta n_{sat}(x,z) = n_\infty \left[1 - \frac{1}{(1+I(x,z)/I_{sat})^p}\right], \quad (1)$$

where the corresponding Kerr coefficient is such that $n_2 = n_\infty p/I_{sat}$, with p being the saturation index related to the light beam intensity power. Numerical solutions for the NLS equation in presence of the above term were discussed for $p = 1$ [54]. Additionally, exact bright solitons were derived for $p = 2$ [55–58], and more recently, dark and bright solitons were derived for $p = 2$ and $p = 3$ [59]. The nonlinear dynamics of a periodically perturbed second-order ordinary differential equation was also recently addressed through traveling wave variables in a saturable NLS model for $p = 2$ [60]. Obviously, the generalized expression given by Eq. (1) offers the possibility to tune the saturation index with the possible generation of a broad range of nonlinear structures. That is the main motivation of the present investigations since the propagation of intense continuous waves in dielectric media leads to several major nonlinear phenomena having fundamental interests and practical applications. A well-known example of those phenomena is the modulational instability (MI), which arises from the interplay between dispersive and nonlinear effects and manifests itself in the exponential growth of weak perturbations [61, 62]. The gain leads to amplification of sidebands, which break up the otherwise uniform wave and generate fine localized structures. Thus, it may act as a precursor for the formation of solitons. The phenomenon of MI has been identified and studied in various physical systems, such as fluids [63], plasmas [64–66], nonlinear optics [67–69], metamaterials [70, 71], discrete nonlinear systems [72–75], and BECs [76–79], to cite a few. It has been shown that MI is strongly affected by mechanisms such as saturation of nonlinearity [80], coherence properties of optical beams [81], linear and nonlinear gratings [82], and generation of super-continuum spectra [83], and so on. Interestingly, the first experimental studies of MI in a nonlocal medium were reported by Peccianti et al. [84], where nematic liquid crystals were

used. They showed that due to their inherent orientational nonlocal nonlinearity, the sign-definite exponential response can efficiently contribute to quenching the MI. Albeit the same remark was made in other physical settings, the question related to the coupled influence of nonlocal and saturable nonlinearities remains unmarked, especially in the context of MI, when there is a possibility of parametrically playing on the index of saturation. Such a question is exclusively addressed in the present paper. In this paper, we show that the quenching effect of the nonlocal nonlinearity on the MI is corrected by the presence of the saturable nonlinearity, especially when the saturable index and the nonlocality range are well-balanced.

The rest of the paper is outlined as follows: in Section II, we first introduce the proposed model and thereafter proceed to the linear stability analysis of MI. An expression for the growth rate of MI is derived and used to discuss the manifestation of MI parametrically. Particular attention is given to the impact of the saturation index, the nonlocality parameter, the input power, and the nonlinearity strengths. Section III presents full numerical results, where the link between the analytical predictions and nonlinear pattern formation, and RWs in particular, is established. The effect of system parameters is explored, especially different combinations of the saturation index and the nonlocality parameter under various nonlinearity strengths. Section IV is devoted to concluding remarks.

II. MODEL AND MODULATIONAL INSTABILITY PROCESS

The dynamics of optical pulses in the regime of slowly varying envelope amplitude is usually described by an NLS equation that includes both dispersion and nonlinearity. For the case of instantaneous response, it is written in the form

$$iq_z + q_{xx} + \Delta n(x,z)q(x,z) = 0, \tag{2}$$

where $q(x,z)$ is the complex envelope amplitude of the pulse, with x and z representing transverse and longitudinal coordinates, respectively. As is well-known, in nonlinear Kerr media, the intensity-dependent refractive index change is given by $\Delta n(x,z) = I(x,z)$, with the intensity of the beam $I = |q(x,z)|^2$. In the case of nonlinear media with competing nonlocal and saturable nonlinearities, the nonlinear refractive index change of the medium can be represented by the following phenomenological model

$$\begin{aligned}\Delta n(x,I) &= \Delta n_1(x,z) + \Delta n_2(x,z)\\ &= \alpha\int_{-\infty}^{+\infty} R(x-x^{'})I(x',z)dx^{'}\\ &\quad - m\left[q - \frac{q}{(1+aI(x,z))^p}\right],\end{aligned} \tag{3}$$

where α represents the strength of the nonlocal cubic nonlinearity, $m = n_\infty$ is the nonlinear saturation coefficient, $a = 1/I_{sat} \neq 0$ is the saturation intensity, p is the power of the intensity of the light beam or saturation index, and the minus sign indicates self-defocusing interaction. Introducing Eq. (3) into Eq. (2), one obtains the following nonlocal and saturable NLS equation governing the evolution of the beam [9, 59]:

$$\begin{aligned}iq_z + q_{xx} + \alpha q\int_{-\infty}^{+\infty} R(x-x^{'})|q(x^{'},z)|^2dx^{'}\\ - m\left[q - \frac{q}{(1+a|q|^2)^p}\right] = 0.\end{aligned} \tag{4}$$

The form of the convolution integral represents the nonlocal nonlinear response. Typically, the response functions are either exponential (as in liquid crystals) or Gaussians [85]. Below, we assume the latter by setting

$$R(x) = \frac{1}{\sigma\sqrt{\pi}}\exp\left[-\frac{x^2}{\sigma^2}\right], \tag{5}$$

where the coefficient σ determines the corresponding nonlocality ranges of the cubic nonlinearity, while the coefficient in front of the Gaussians follows from the normalization condition, $\int_{-\infty}^{+\infty} R(x)dx = 1$. In the case of the Gaussian nonlocal response function, the Fourier transform is given by

$$\hat{R}(k) = \exp\left[-\frac{1}{4}\sigma^2k^2\right]. \tag{6}$$

The saturable nonlocal NLS Eq. (4) permits exact plane wave solutions of the form:

$$q(z,x) = \sqrt{P_0}e^{i(k_0x-\omega_0z)}, \tag{7}$$

where P_0, k_0, and ω_0 are linked through the nonlinear dispersion relation

$$\omega_0 = k_0^2 - \alpha P_0 + \frac{mapP_0}{(1+aP_0)^p}. \tag{8}$$

The stability of the steady state can be examined by introducing a perturbed field by assuming that

$$q(z,x) = \left[\sqrt{P_0} + u(z,x)\right]e^{i(k_0x-\omega_0z)}, \tag{9}$$

with $u(z,x)$ being a small complex modulation. Substituting Eq. (9) into Eq. (4) and linearizing about the plane wave (7), we get a linear equation for $u(z,x)$:

$$\begin{aligned}iu_z + u_{xx} + 2\alpha P_0\int_{-\infty}^{+\infty} R(x-x^{'})\Re\{u(z,x^{'})\}dx^{'}\\ - \frac{2mapP_0}{(1+aP_0)^p}\Re\{u(z,x)\} = 0,\end{aligned} \tag{10}$$

where $\Re\{u(z,x)\}$ represents the real part of $u(z,x)$.

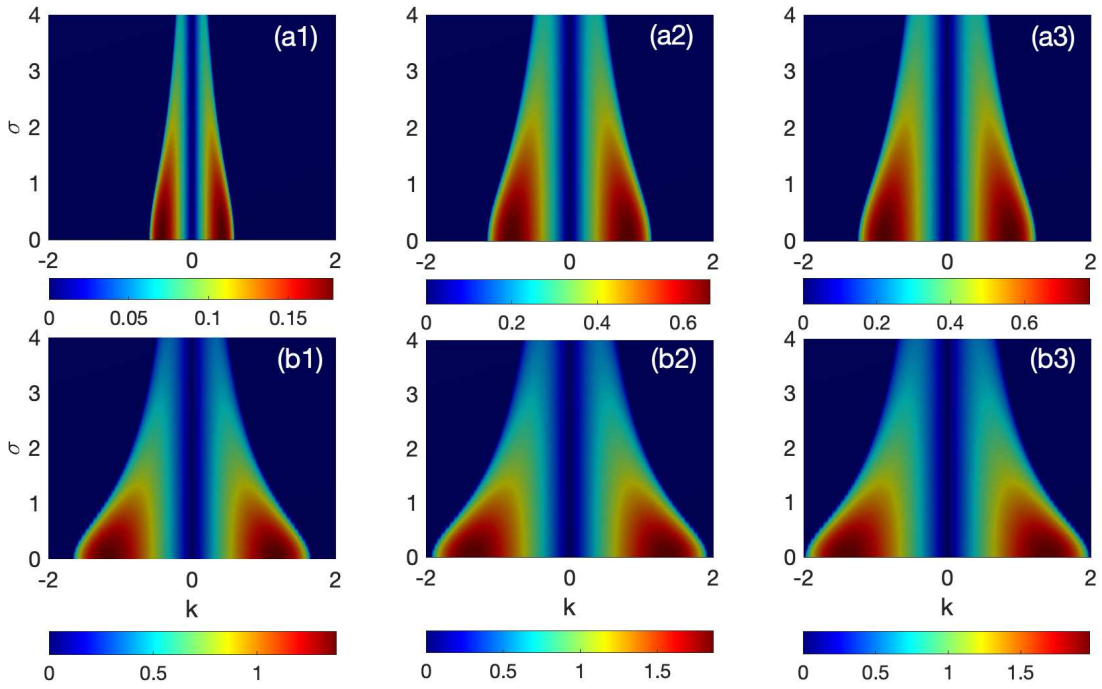

Figure 1: The panels show the MI growth rate spectra under the competition between the nonlocal nonlinearity and the saturable nonlinearity with $\alpha = 0.4$ (panel (aj)$_{j=1-3}$) and $\alpha = 1$ (panels (bj)$_{j=1-3}$). The other parameter values are such that $m = 0.8$, $P_0 = 2$ and $a = 2$, and the saturation index taking the respective values $p = 1$, $p = 2$ and $p = 3$, corresponding to columns from left to right.

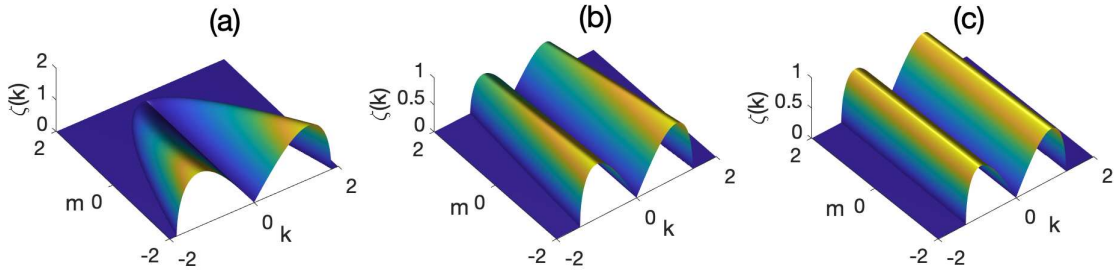

Figure 2: The panels show the MI growth rate versus the wavenumber k and the nonlinear parameter m for: (a) $p = 1$, (b) $p = 2$ and (c) $p = 3$, with $\alpha = 0.4$, $a = 2$, $P_0 = 2$, and $\sigma = 0.1$.

Decomposing the perturbation u into real and imaginary parts, $u = u_r + iu_i$, we obtain two coupled equations

$$\frac{\partial u_r}{\partial z} + \frac{\partial^2 u_i}{\partial x^2} = 0, \tag{11a}$$

$$\frac{\partial u_i}{\partial z} - \frac{\partial^2 u_r}{\partial x^2} - 2\alpha P_0 \int_{-\infty}^{+\infty} R(x - x')u_r(z, x')dx' + \frac{2mapP_0}{(1 + aP_0)^p} u_r(z, x) = 0. \tag{11b}$$

By introducing the Fourier transforms

$$\begin{aligned} \hat{u}_r &= \int_{-\infty}^{+\infty} u_r \exp(ikx)dx, \\ \hat{u}_i &= \int_{-\infty}^{+\infty} u_i \exp(ikx)dx, \\ \hat{R}(k) &= \int_{-\infty}^{+\infty} R(x) \exp(ikx)dx, \end{aligned} \tag{12}$$

where $\hat{R}(k)$ is the Fourier spectrum of $R(x)$, $\hat{u}_r$ is the Fourier transform of u_r, and $\hat{u}_i$ is the Fourier transform of u_I, respectively. Exploiting the convolution theorem for Fourier transforms, the linearized system is converted

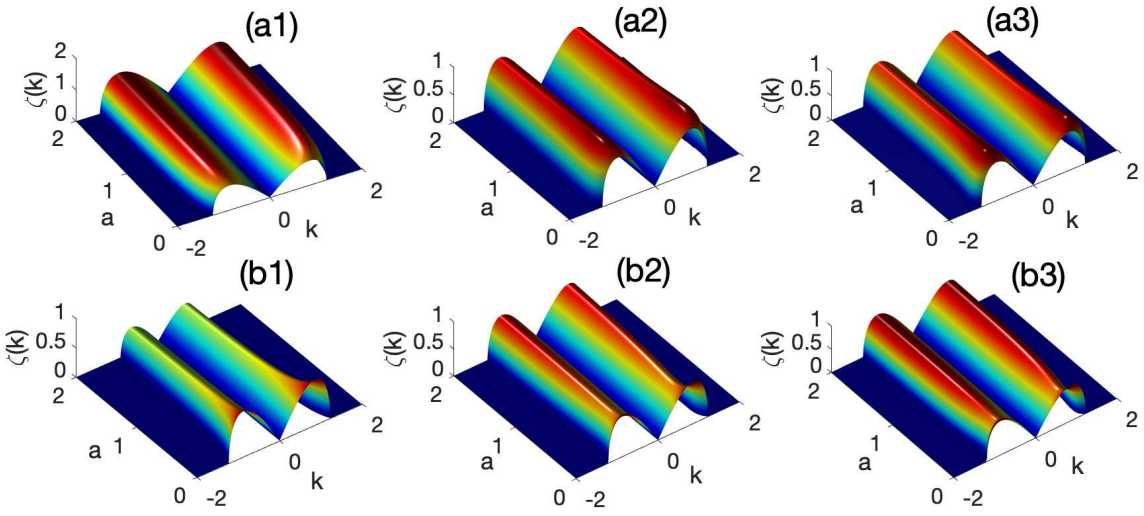

Figure 3: The panels show the MI growth rate versus the wavenumber k and the nonlinear parameter a for: $(\mathrm{aj})_{j=1-3}$ $m=-0.8$, $(\mathrm{bj})_{j=1-3}$ $m=0.8$, from left to right, columns correspond to $p=1$, $p=2$ and $p=3$, with $\alpha=0.4$, $p_0=2$, and $\sigma=0.1$.

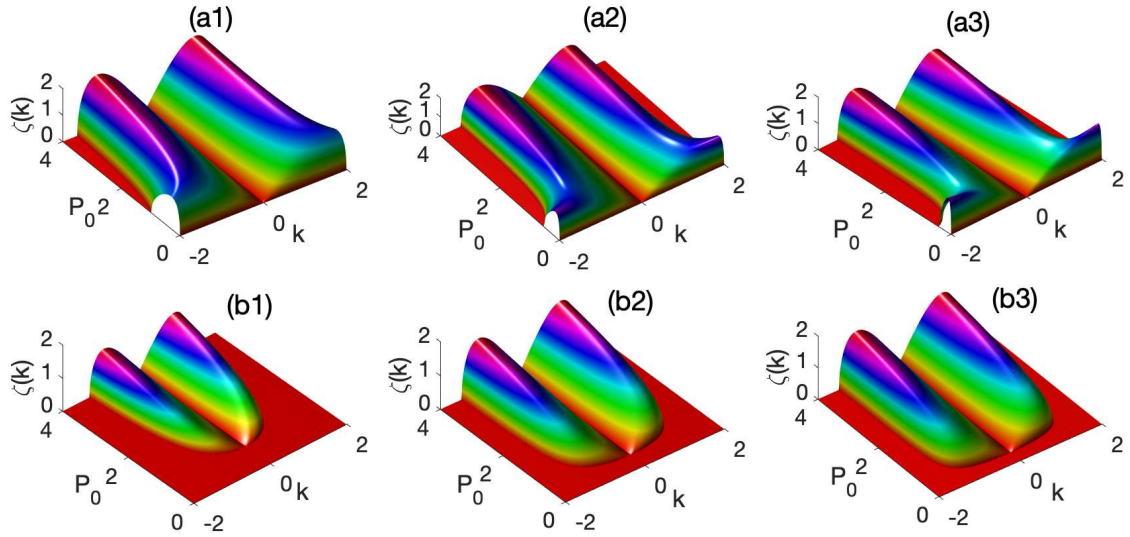

Figure 4: The panels show the MI growth rate versus the wavenumber k and the input power P_0. Panels $(\mathrm{aj})_{j=1-3}$ $m=-0.8$ and panels $(\mathrm{bj})_{j=1-3}$ $m=0.8$, with columns from left to right corresponding to $p=1$, $p=2$ and $p=3$, and $\alpha=0.4$, $\sigma=0.1$.

to a set of ordinary differential equations in k space

$$\begin{aligned}\frac{\partial \hat{u}_r}{\partial z}-k^2\hat{u}_i=0,\\ \frac{\partial \hat{u}_i}{\partial z}+k^2\hat{u}_r-2\alpha P_0\hat{R}\hat{u}_r+\frac{2mapP_0}{(1+aP_0)^p}\hat{u}_r=0,\end{aligned}\tag{13}$$

which can be written in the following compact matrix form

$$\partial_z \underline{X}=A\underline{X},\tag{14}$$

where the vector $\underline{X}$ and the matrix A are defined as

$$\begin{aligned}\underline{X}&=\begin{pmatrix}\hat{u}_r\\ \hat{u}_i\end{pmatrix},\\ A&=\begin{pmatrix}0 & k^2\\ -k^2+2\alpha P_0\hat{R}(k)-\frac{2mapP_0}{(1+aP_0)^p} & 0\end{pmatrix}.\end{aligned}\tag{15}$$

The eigenvalues λ of the matrix A are given by

$$\lambda^2=-k^2P_0\left[\theta k^2-2\left(\alpha\hat{R}(k)-\frac{map}{(1+aP_0)^p}\right)\right],\tag{16}$$

where we have defined $\theta=1/P_0$, with k denoting the wavenumber. The general dispersion relation (16) consti-

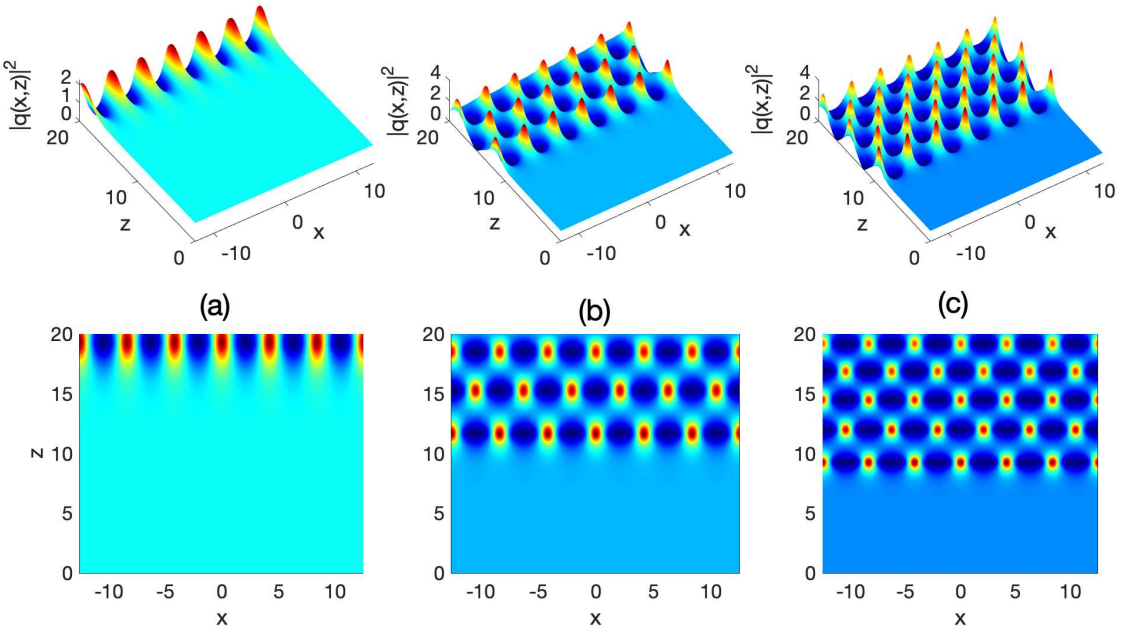

Figure 5: Propagation of the perturbed plane wave intensity and wave pattern formation under the strong influence of the nonlocal nonlinearity, i.e., $\alpha > m$, with $p = 1$, $P_0 = 1$, $k = 0.75$, $a = 0.2$, $m = 0.1$ and $\sigma = 0.5$. Panels (a), (b) and (c) correspond, respectively to values $\alpha = 0.8$, $\alpha = 1.2$ and $\alpha = 2$ of the cubic nonlinearity coefficient.

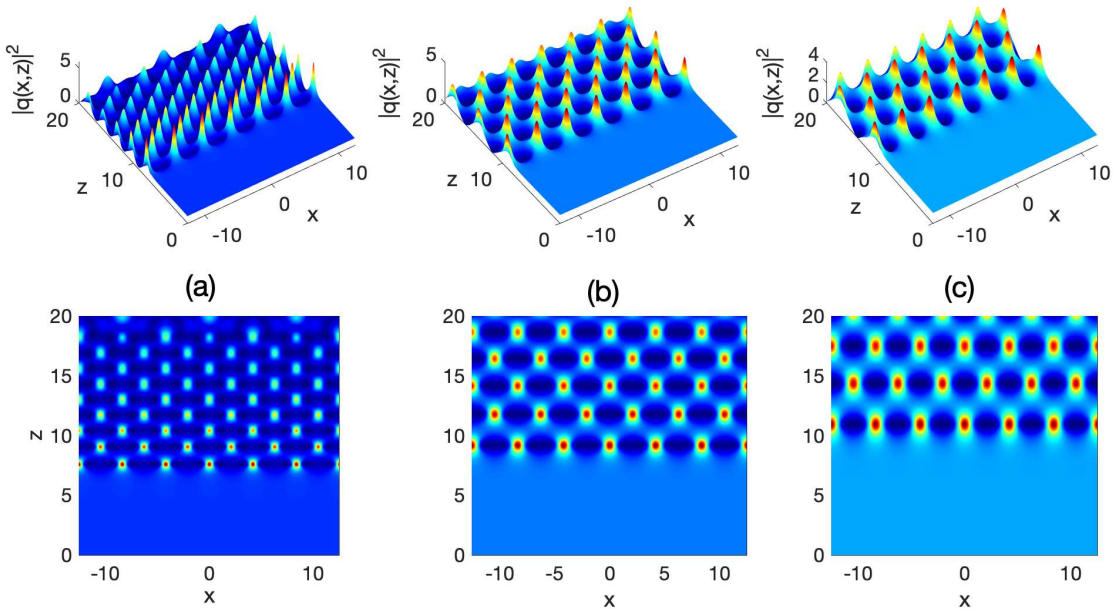

Figure 6: Propagation of the perturbed plane wave intensity and development of MI under strong influence of the nonlocal nonlinearity, i.e., $\alpha > m$, with $p = 1$, $P_0 = 1$, $k = 0.75$, $a = 0.2$, $m = 0.1$ and $\alpha = 1.2$. Panels (a), (b) and (c) correspond, respectively to values $\sigma = 0.4$, $\sigma = 0.6$ and $\sigma = 0.8$ of the non locality parameter.

tutes the basis of our study of MI. Therefore, plane-wave solutions are stable if perturbations at any wavenumber k do not grow with propagation. This is the case as long as λ is purely imaginary. Physically, modulational stability means that small-amplitude waves can propagate along with the background intense plane wave, although their propagation parameter λ depends on the plane wave intensity P_0. Since $k^2 P_0 > 0$, plane wave solution are unstable if

$$\theta k^2 - 2\left(\alpha \hat{R}(k) - \frac{map}{(1+aP_0)^p}\right) < 0. \tag{17}$$

The MI gain is defined as the positive real part of the eigenvalue λ, i.e.,

$$\zeta(k) = |k|\sqrt{P_0}\left|\Re\left\{\sqrt{2\left(\alpha\hat{R} - \frac{map}{(1+aP_0)^p}\right) - \theta k^2}\right\}\right|, \tag{18}$$

where $\Re\{\cdot\}$ indicates the real part of an expression.

The panels of Fig. 1 show, for example, the dependence of the MI growth rate on the wavenumber k and the nonlocality parameter σ. In general, the instability spectrum is manifested by a set of symmetrical lobes, with a maximum growth rate for small values of σ. When σ increases, the instability tends to disappear. Another significant effect is related to the strength of the nonlocal nonlinearity coefficient α, confronted with the strength of the saturable nonlinearity coefficient m. In fact, for $m = 0.8$, α takes the value 0.4 in Fig. 1(aj)$_{j=1-3}$ and 1 in Fig. 1(bj)$_{j=1-3}$. With increasing the saturation index p, the bandwidth of instability increases and covers large intervals of the wavenumber k, especially when $\alpha > m$. While the defocusing case ($\alpha < 0$) offers marginal modulation stability [85, 86], it is shown in Fig. 2 that the saturation strength m takes both positive and negative values, with the possibility of instability when the saturation index p changes. For $p = 1$, negative values of m offer the maximum growth rate of instability that decreases with m and disappears. However, the cases $p = 2$ and $p = 3$ show a continuous MI growth rate for all values of m, even though the bandwidth and intensity decrease. In the context where the advantage is given to the saturation nonlinearity ($\alpha = 0.1$), the saturation parameter a importantly modifies the growth rate spectrum both when $m = -0.8$ [see Fig. 3(aj)] and $m = 0.8$ [see Fig. 3(bj)]. In the first case, increasing the saturation index p reduces the growth rate intensity and creates humps of high growth rate for small values of a. In the second case, the instability windows start with a high growth rate that drops and expands more when p increases. Following the same procedure as in Fig. 3, the input power, combined with the wavenumber k, also offers some windows of instability that are very sensitive to competition between the nonlocal and the saturating nonlinearities via the coefficients α and m, respectively, under the impact of the saturation index p. Results corresponding to $m = -0.8$ and $\alpha = 0.4$ are reported in Fig. 4(aj), where the instability growth rate is

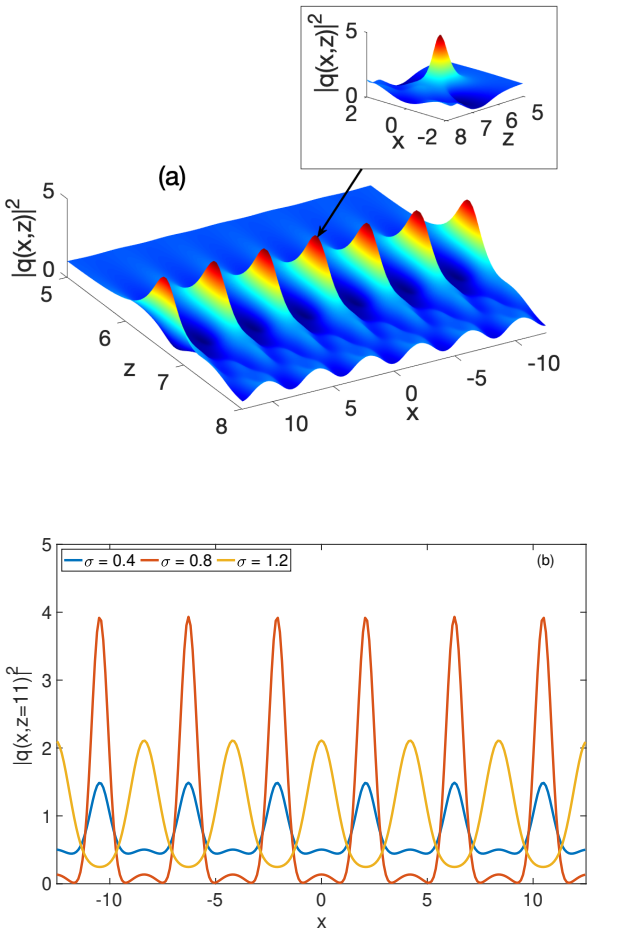

Figure 7: Panel (a) show a section of Fig. 6 confirming individual object to be RWs. This is further supported by the inset that displays the structure of such individual objects whose train forms an Akhmediev breather. Panel (b) shows the impact of the nonlocality parameter σ on the characteristics of the MI, along with the subsequent emergence of RWs for lower values of σ.

an increasing function of the input power P_0, with the wavenumber bandwidth being distributed between two lobes of instability. With increasing the saturation index p, the instability bandwidth along the $k-$axis shrinks, while the window of instability offered by small values of P_0 tends to close. The scenario offered by $m = 0.8$, with α keeping the same value, rather shows symmetrical lobes that expand the instability bandwidth when p increases, with the bandgap given by small values of P_0 getting extended to $P_0 \to 0$. Even in this particular case, $\zeta(k)$ is an increasing function of the input power P_0.

III. NUMERICAL EXPERIMENT

One of the previous section's main objectives was determining regions of parameters where combined nonlocal and saturable nonlinearities can balance with disper-

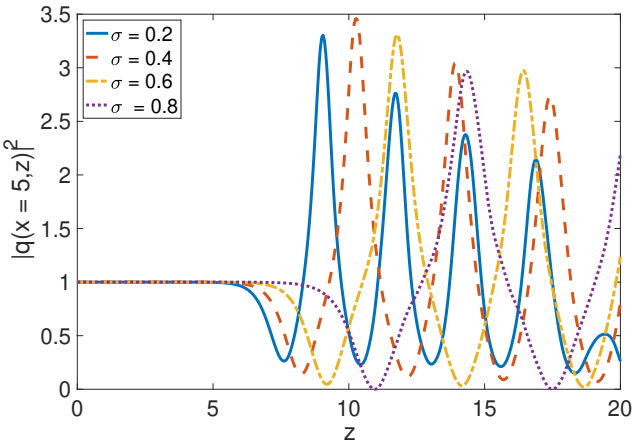

Figure 8: The panel summarizes the effect of the nonlocality parameter σ on the development of MI under the strong effect of the nonlocal nonlinearity ($\alpha > m$), with parameter values $p = 1$, $P_0 = 1$, $k = 0.75$, $a = 0.2$, $m = 0.1$ and $\alpha = 1.2$.

sion and give rise to modulated waves and nonlinear patterns. Obviously, the linear stability analysis does not say anything about the long-time evolution of the CW, which requires direct numerical simulations to be validated. Therefore, for the completeness of our study, the set of equations (4) has been integrated using the split-step Fourier method. An initial signal input of the form

$$q(x, z = 0) = \sqrt{P_0} + \varepsilon \cos(kx), \tag{19}$$

has been injected, with $k = 0.75$, $\varepsilon = 10^{-4}$ and $P_0 = 1$, values that are supposed to support the development of MI. Moreover, the results are extracted in terms of the signal intensity $I = |q(x, z)|^2$, where attention is mainly paid to the competition between the nonlinear and saturable nonlinearities in the generation of modulated waves.

As stress so far, one of the advantages of the studied system is the tunable saturable nonlinearity through the index p, which is given the values $p = 1$, 2 and 3 in the rest of this paper. On the other hand, the originality of the present contribution also lies in the inclusion of the nonlocal Kerr nonlinearity that is manifested by the two parameters α and σ. In a situation where the nonlocal nonlinearity is slightly predominant, i.e., $\alpha > m$, one obtained the features of Fig. 5, where wave patterns and their corresponding density plots highlight the impact of the cubic nonlinearity coefficient. Although the value $\alpha = 0.8$ supports the plane wave stability, decreasing α delays the occurrence of MI. Interestingly, the chosen values of parameters support wave modulation for $\alpha = 1.2$ and $\alpha = 2$, which shows a good agreement between our analytical predictions and the numerics. Beyond the described features, one may notice an increase in wave intensity when α increases. Under the same conditions where the nonlocal nonlinearity is predominant, the effect of the nonlocality parameter σ is addressed in Fig. 6, for $\alpha = 1.6$. From panels (a) to (c), it is ostensible that increasing σ produces a contrary effect, i.e., delayed formation of patterns under MI. In the process, the solitonic objects are more localized; their intensity drops for higher values of σ, which corroborates the finding of Fig. 1, from which high values of σ drop the growth rate and tend to quench instability. This latter aspect can be clearly appreciated in Fig. 8, where increasing values of σ delay MI and reduce the amplitude of the wave train with propagation distance increasing. On exploring individual objects closely, one notices their similarity with RWs, where a train displayed against the space displays an Akhmediev breather [see Fig. 7(a)]. Confirmation is further given in panel (b) of Fig. 7, in which lower values of the nonlocality parameter support the occurrence of RWs, showing their straightforward relationship with the occurrence of MI. This is not, therefore, a surprise but instead reinforces the fact that the exact solutions of the NLS equation that describes the nonlinear mode of MI are the Akhmediev breathers. However, beyond the MI excitation, other linear and nonlinear underlying physical processes can drive the emergence of RWs, among which are the integrable turbulence [87, 88], supercontinuum generation [89], optical filamentation [90], asymmetry, and inhomogeneity [91], supercontinuum generation [89]. Of course, the strong link between the occurrence of MI and the regime of several recurrences of nonlinear optical waves was experimentally addressed in the seminal work by Pierangeli et al. [92], where it was additionally demonstrated that the recurrent behavior vanishes as integrability is lost and that the complex evolution of the exact initial condition can be accurately predicted in experimental conditions leading to its reconstruction after several return cycles. Along the same line, a novel non-destructive technique was experimentally proposed as a critical tool to characterize mixing processes, new RW formation regimes, and wave turbulence in the optical fiber [93]. Besides, it was shown by Soto-Crespo et al. [94] that there are two ways of adiabatic transformations of a plane wave solution into a train of pulses, with the possibility of explicitly differentiating the A-type Akhmediev breather from the B-type one. Indubitable, from that nomenclature, the Akhmediev breather constituting the patterns in Figs. 5 and 6 are of A-type.

Before going further, let us mention that the effect of the saturable nonlinear response is governed by three important parameters, m, Γ, and p. In previous contributions, the effect of the saturation index taking the values 1 and 2 has been studied both in the context of MI and exact soliton solutions [56, 57]. Here, it appears to be a key parameter that can be used to regulate the saturation effect as witnessed by the features of Figs. 9 and 10. In Fig. 9, where $m = -0.8$, the instability is characterized by a train of coupled modulated waves with a solitonic shape. In general, for $p = 1$, the modulated impulses identically travel along with the distance z, forming a series of wave packets that tend to lose intensity along with the propagation distance. The latter

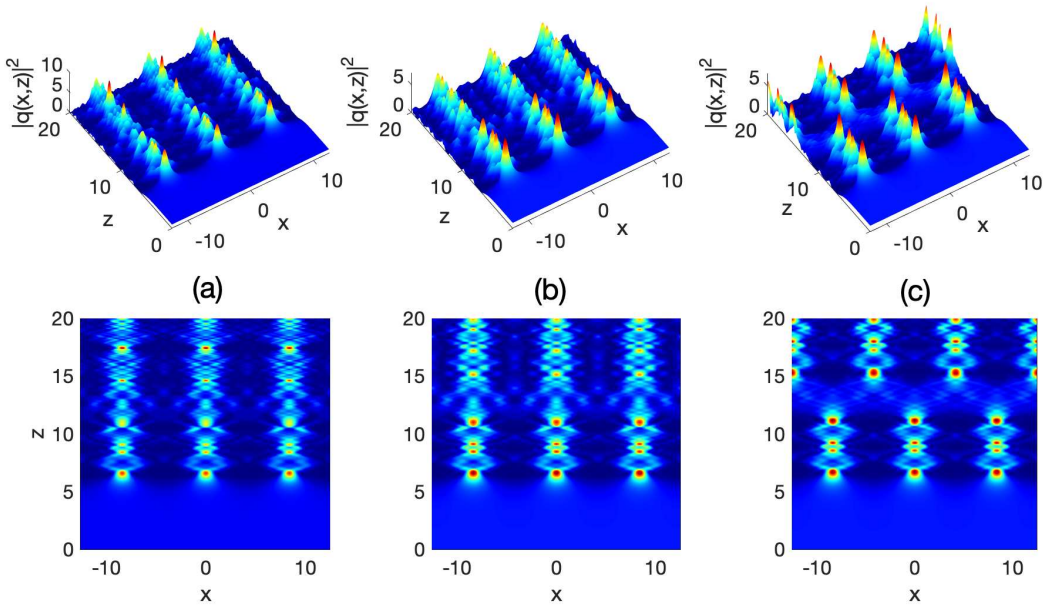

Figure 9: Propagation of the perturbed plane wave intensity and MI development for $\alpha = 0.8$ and $m = -0.8$, with $a = 2$, $p = 1$, $P_0 = 1$, $k = 0.75$, and $\sigma = 2$. Panels (a), (b) and (c) showing wave propagation with corresponding density plots are obtained for the saturation index taking the respective values $p = 1$, $p = 2$ and $p = 3$.

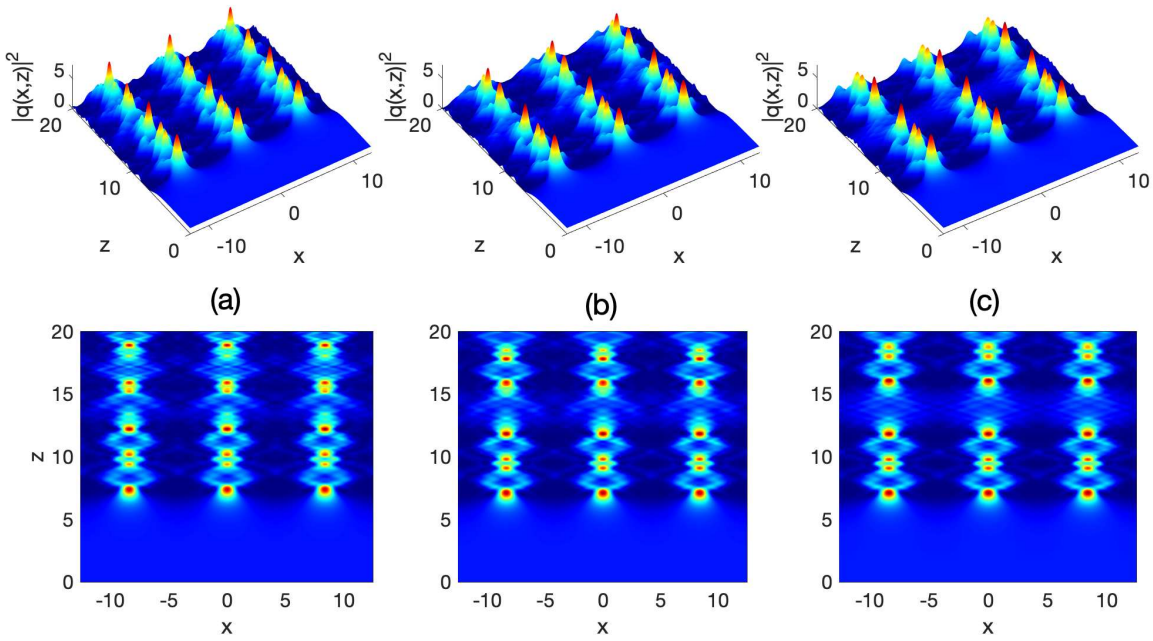

Figure 10: Propagation of the perturbed plane wave intensity and MI development for $\alpha = 0.8$ and $m = 0.8$, with $a = 2$, $p = 1$, $P_0 = 1$, $k = 0.75$, and $\sigma = 2$. Panels (a), (b) and (c) showing wave propagation with corresponding density plots are obtained for the saturation index taking the respective values $p = 1$, $p = 2$ and $p = 3$.

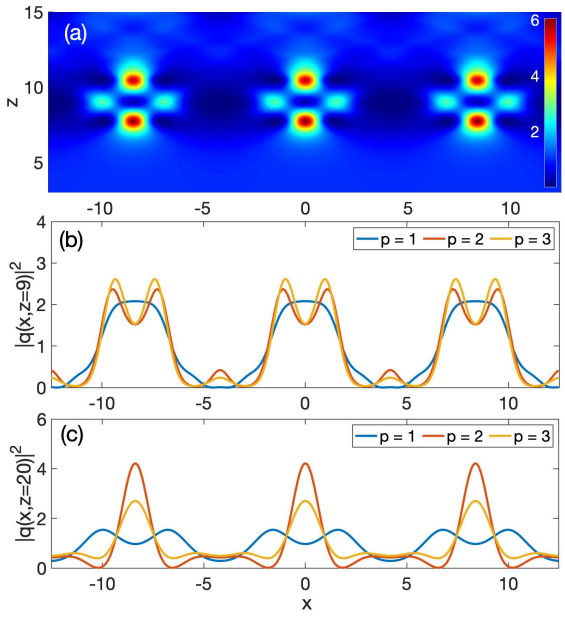

Figure 11: Panel (a) shows a section of the density plot of the wave patterns of Fig. 10, where a train of solitonic molecules is displayed. For different values of the saturation index p, the spatial section, at a distance $z = 9$, of panel (a) is shown in panel (b), where p is revealed to influence the shape of the train at that specific position. For a longer propagation distance, still with p changing, one gets the features of panel (c), where values 2 and 3 of the saturation index lead to RWs at distance $z = 3$, with the other parameter values being: $\alpha = 0.8$ and $m = 0.8$, with $a = 2$, $P_0 = 1$, $k = 0.75$, and $\sigma = 2$.

behavior appears earlier when the saturation index is set to $p = 2$, for which the erratic signal takes over from $z = 12$. Noticeably, increasing p also causes the signal intensity to decrease. Albeit the same behavior is shared by Fig. 9(c), the strong nonlocality, confronted with the negative value of m, changes the propagation features of the signal, which, after $z = 12$, is described by two symmetric trains of solitons and lateral waves at the boundaries. Of course, such behaviors could not also be predicted by the linear stability analysis but agree well with its predictions based on the chosen parameters. Contrary to the previous observations, the patterns of Fig. 10, corresponding to $m = 0.8$, do not display any significant intensity drop and keep the same characteristics. However, for $p = 3$, the generated impulses of solitonic waves are more separated into sequences of wave molecules as depicted in Fig. 10(c). This occurs at a distance $z = 12$ and justifies the spectrum of behaviors already displayed by Fig. 9(c). Obviously, the sign of the saturation coefficient, when well balanced with the nonlocal nonlinear coefficient, can regulate the spatial and distance distribution of the generated patterns. Moreover, the tunability of the saturating nonlinearity, through the index p, gives a direct way to produce richer behaviors of the optical signal, which earlier calculations could not support, therefore showing the advantage of the proposed model, which under other nonlocal response functions may support more exotic behaviors and give more insights for experimental investigations. This particular scenario is summarized in Fig. 11, where panel (a) shows a section of the molecular structures forming the trains. At propagation distance $z = 9$, the same of structures varies depending on the value of the saturation index p as depicted in Fig. 11(b). For $p = 1$, the instability is characterized by a train of extended bell-shaped solitons. The scenario changes when the index p takes the respective values 2 and 3, where one notices the emergence of two-humped soliton trains, with a lower band in-between. Over long-distance propagation, the results displayed in Fig. 11(c) are obtained, where p takes values as previously. Remarkably, for $p = 2$ and $p = 3$, there is a persistence of RW train formation, which confirms their robustness in the studied model. To proceed further, we should also indicate that such Akhmediev breathers were classified as B-type in Ref. [94], where their occurrence was also related to the development of MI. The investigation of the tools to control the shape and the characteristics of such structures has been debated recently, where it was shown that the frequency of the modulation could play a significant role under conditions where coefficients are periodically varying [95]. This could lead to wave compression in some contexts, requiring additional bifurcation theory tools to be predicted and controlled [95]. However, in the present case, combining the nonlocality and controllable saturation also offers the possibility to generate trains of solitons that include several modes, the only requirement being a judicable choice of wave and system parameters. For example, fixing the saturation index $p = 3$, with $m = 2$ and $\alpha = 1.2$, the variation of the nonlocality parameter σ gives rise to the features of Fig. 12, where wave modulation adopts different behaviors as σ increases.

It is well-known that the current manufacturing material of fiber optic strands is made from plastic or glass (Silica), depending on the requirement. Due to the advancement of fiber optic technology, several research teams have concentrated their efforts on designing optical fibers with nonsilica glasses, including tellurite [96] or chalcogenide glasses [97], to name a few. The interest in such glasses relies on their specific properties that are significantly different from those of silica. Their particularity is due to their high nonlinear indices that originate from high refractive indices, leading to nonlinear coefficients higher than that of silica. Complex nonlinear expressions mathematically give this for the refractive index that can be polynomial or saturable. In doing so, models including saturable nonlinearity provide a good description of the features of optical glass materials far from resonance. In the context where pump powers are high, leading to large nonlinear absorption with complicated practical applications, a relatively moderate nonlinear absorption[98, 99] may be provided by a saturation of the cubic nonlinearity of sulfide and heavy-metal oxide

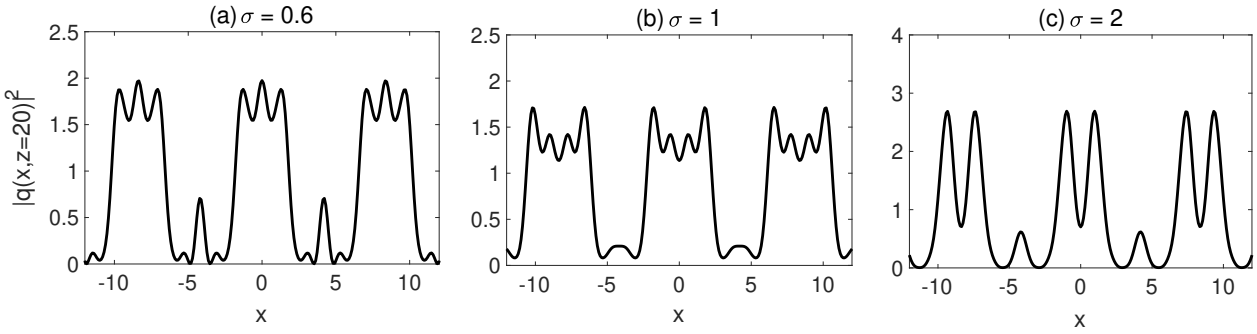

Figure 12: The panels show the output signal intensity versus space for different values of the nonlocality parameter σ. The dynamical features shows the emergence of different modes corresponding to the value of σ in the context of Fig. 9, with other parameter values being: $\alpha = 0.8$ and $m = 0.8$, with $a = 2$, $p = 3$, $P_0 = 1$, and $k = 0.75$.

glasses. It has, in fact, been demonstrated experimentally that sulfide and heavy-metal oxide glasses could satisfactorily replace semiconductor-doped glasses for effective practical applications when absorption constitutes a serious drawback [100, 101]. Such enhanced properties of suitable nonlinearly saturable materials require improved models that picture their tunability, conditioned by an adjustable absorption capacity while pumped by photons that are in resonance with no energy level of the core materials. Intrinsically, the nonlinear response of the materials is a more complex function of the light intensity. Interestingly, from the nonlocal z-scan theory, when such optical materials are placed in a certain medium, their nonlinear response can be significantly affected due to the nonlocal properties of the medium [102]. In our case, the materials and the nonlocal medium may then constitute a composite material with specific properties. Examples of such include the incorporation of Au nanoparticles that can significantly enhance the nonlinear optical properties of graphene oxide [102]. More recently, castor oil was also listed as a promising nonlinear medium due to its interesting nonlocal properties that can boost the optical features of materials, such as absorptive properties of nanoparticles for optical applications [103]. Moreover, it is a well-known fact that the range of nonlocality is naturally adjusted by saturation effects, like in photorefractives where the Debye length tunes the strength of nonlocality [104] and liquid crystals where the orientation molecules angle has a maximum value [105]. Our work, therefore, suggests the experimental realization of the MI process on glass with combined inherent optical, and thermal nonlinearity in which the absorption of the incident perturbed CW is relatively moderated, providing a favorable ground for the manifestation of saturation, where increasing the power P_0, after adjusting the saturation index p and the range of nonlocality σ, can cause the CW to disintegrate into structures of any types depending on the nonlinearity strengths α and m.

IV. CONCLUDING REMARKS

This paper's primary purpose was to analyze MI's properties in an extended nonlinear medium with controllable saturation and nonlocal cubic nonlinearity. Using the linear stability analysis, an expression for the MI growth rate has been derived, and we have investigated the competitive effects between the nonlocal cubic nonlinearity and saturation using tools like the nonlinearity coefficients α and m, the saturation index p and the nonlocality parameter σ under Gaussian nonlocal response. The MI growth rate is sensitive to changes in such parameters, interchangeably under saturation and nonlocality domination. Moreover, it has been found that high values of the nonlocality parameter tend to quench instability. In contrast, when the saturation index increases, high input power values tend to amplify the instability through enlarged wavenumber bandwidth. The analytical predictions have been assessed via direct numerical simulations, where the activation of MI has been confirmed to trigger pattern formation through the emergence of RWs, namely A- and B-types Akhmediev breathers, and other exotic types of solitonic molecules. The robustness of such in the proposed model has been tested using parameter variations, especially the nonlocality parameter, the saturation coefficient, and the saturation index. We have also demonstrated that in the context where the saturation parameter is well-tuned, increasing the nonlocality parameter does not quench instability but rather gives rise to a broad range of modes whose characterization and application may be a starting point for experimental control and manipulation of soliton dynamics in the proposed saturable model.

Acknowledgements

CBT thanks the Kavli Institute for Theoretical Physics (KITP), University of California Santa Barbara (USA), where this work was supported in part by the National

Science Foundation Grant no.**NSF PHY-1748958**, NIH Grant no.**R25GM067110**, and the Gordon and Betty Moore Foundation Grant no.**2919.01**.

[1] Y. S. Kivshar and G.P. Agrawal, *Optical Solitons: From Fibers to Photonic Crystals* (Academic Press, San Diego, CA, USA, 2003).

[2] L.P. Pitaevskii and S. Stringari, *Bose-Einstein Condensation* (Oxford University Press, Oxford, UK, 2003).

[3] S.H. Schochet and M.I. Weinstein, Commun. Math. Phys. **106**, 569 (1986).

[4] P. P. Kiran, B. N. S. Bhaktha, D. N. Rao, and G. De, J. Appl. Phys. **96**, 6717 (2004).

[5] Y. X. Zhang and Y. H. Wang, RSC Adv. **7**, 45129 (2017).

[6] A. S. Reyna, K. C. Jorge, and C. B. de Araújo, Phys. Rev. A **90**, 063835 (2014).

[7] A. Griesmaier, J. Stuhler, T. Koch, M. Fattori, T. Pfau, and S. Giovanazzi, Phys. Rev. Lett. **97**, 250402 (2006).

[8] M. Warenghem, J. F. Blach, and J. F. Henninot, J. Opt. Soc. Am. B **25**, 1882 (2008).

[9] W. Krolikowski, O. Bang, N. I. Nikolov, D. Neshev, J. Wyller, J. J. Rasmussen, and D. Edmundson, J. Opt. B: Quant. Semiclas. Opt. **6**, S288 (2004).

[10] W. Krolikowski, O. Bang, J. J. Rasmussen, and J. Wyller, Phys. Rev. E **64**, 016612 (2001).

[11] J. Wyller, W. Krolikowski, O. Bang, and J. J. Rasmussen, Phys. Rev. E **66**, 066615 (2002).

[12] Y. Y. Lin, R.-K. Lee, and Yu. S. Kivshar, J. Opt. Soc. Am. B **25**, 576 (2008)

[13] F. Ye, Y. V. Kartashov, and L. Torner, Phys. Rev. A **77**, 043821 (2008).

[14] Y. V. Kartashov, V. A. Vysloukh, and L. Torner, Phys. Rev. Lett. **93**, 153903 (2004).

[15] B. D. Skuse and N. F. Smyth, Phys. Rev. A **77**, 013817 (2008).

[16] M. Shen, Q. Kong, C.-C. Jeng, L.-J. Ge, R.-K. Lee, and W. Krolikowski, Phys. Rev. A **83**, 023825 (2011).

[17] C. Rotschild, B. Alfassi, O. Cohen, and M. Segev, Nat. Phys. **2**, 769 (2006).

[18] C. Rotschild, O. Cohen, O. Manela, M. Segev, and T. Carmon, Phys. Rev. Lett. **95**, 213904 (2005).

[19] M. Peccianti, C. Conti, G. Assanto, A. D. Luca, and C. Umeron, Nature **432**, 733 (2004).

[20] S. Skupin, M. Saffman, and W. Krolikowski, Phys. Rev. Lett. **98**, 263902 (2007).

[21] P. Pedri and L. Santos, Phys. Rev. Lett. **95**, 200404 (2005).

[22] C. R. Rosberg, F. H. Bennet, D. N. Neshev, P. D. Rasmussen, O. Bang, W. Krolikowski, A. Bjarklev, and Y. S. Kivshar, Opt. Exp. **15**, 12145 (2007).

[23] P. D. Rasmussen, F. H. Bennet, D. N. Neshev, A. A. Sukhorukov, C. R. Rosberg, W. Krolikowski, O. Bang, and Y. S. Kivshar, Opt. Lett. **34**, 295 (2009).

[24] N. I. Nikolov, D. Neshev, O. Bang, and W. Krolikowski, Phys. Rev. E **68**, 036614 (2003).

[25] M. Bache, O. Bang, J. Moses, and F. W. Wise, Opt. Lett. **32**, 2490 (2007).

[26] C. Conti, S. Trillo, G. Valiulis, A. Piskarskas, O. Jedrkiewicz, J. Trull, and P. Di Trapani, Phys. Rev. Lett. **90**, 170406 (2003).

[27] M. Bache, O. Bang, W. Krolikowski, J. Moses, and F. W. Wise, Opt. Exp. **16**, 3273 (2008).

[28] H. Xu, C. Hang, and G. Huang, Phys. Rev. A **101**, 053832 (2020).

[29] C. Zhan, D. Zhang, D. Zhu, D. Wang, Y. Li, D. Li, Z. Lu, L. Zhao, and Y. Nie, J. Opt. Soc. Am. B **19**, 369 (2002).

[30] R.A. Ganeev, M. Baba, M. Morita, A. I. Ryasnyansky, M. Suzuki, M. Turu, and H Kuroda, J. Opt. A: Pure Appl. Opt. **6**, 282 (2004).

[31] E.L. Falcao-Filho, C. B. de Araújo, G. Boudebs, H. Leblond, and V. Skarka, Phys. Rev. Lett. **110**, 013901 (2013).

[32] G. Boudebs, S. Cherukulappurath, H. Leblond, J. Troles, F. Smektala, F. Sanchez, Opt. Commun. **219**, 427 (2003).

[33] K. Ogusu, J. Yamasaki, S. Maeda, M. Kitao, and M. Minakata, Opt. Lett. **29**, 265 (2004).

[34] B. Gu, Y. Wang, W. Ji, and J. Wang, Appl. Phys. Lett. **95**, 041114 (2009).

[35] A.S. Reyna, C.B. de Araujo, Phys. Rev. A **89**, 063803 (2014).

[36] H.A. Garcia, G. B. Correia, R. J. de Oliveira, A. Galembeck, and C. B. de Araújo, J. Opt. Soc. Am. B **29**, 1613 (2012).

[37] S. Giorgini, L. P. Pitaevskii, and S. Stringari, Rev. Mod. Phys. **80**, 1215 (2008).

[38] P. F. Bedaque, E. Braaten, and H. W. Hammer, Phys. Rev. Lett. **85**, 908 (2000).

[39] E. Braaten, H. W. Hammer, and T. Mehen, Phys. Rev. Lett. **88**, 040401 (2002).

[40] M. W. Jack, Phys. Rev. Lett. **89**, 140402 (2002).

[41] F. Kh. Abdullaev, A. Gammal, L. Tomio, and T. Frederico, Phys. Rev. A **63**, 043604 (2001).

[42] C. Chin, R. Grimm, P. Julienne, and E. Tiesinga, Rev. Mod. Phys. **82**, 1225 (2010).

[43] R. H. Enns and S. S. Rangnekar, and A. E. Kaplan, Phys. Rev. A **36**, 1270 (1987).

[44] A. A. Maradudin, *Surface electromagnetic waves,* presented at Second International School on Condensed Matter Physics (Varna, Bulgaria, 1982).

[45] A. Hasegawa and F. Tappert, Appl. Phys. Lett. **23**, 142 (1973).

[46] A. Hasegawa and F. Tappert, Appl. Phys. Lett. **23**, 171 (1973).

[47] D. McMorrow and W.T. Lotshaw, Chem. Phys. Lett. **178**, 69 (1991).

[48] R. Back, G.A. Kenney-Wallace, W.T. Lotshaw, and D. McMorrow, Chem. Phys. Lett. **191**, 423 (1992).

[49] Y. Kodama and A. Hasegawa, IEEE J. Quant. Electr. **QE-23**, 510 (1987).

[50] R. Radhakrishnan and M. Lakshmanan, Phys. Rev. E **54**, 2949 (1996).

[51] M. Hisakado, T. Iizuka, and M. Wadati, J. Phys. Soc. Jpn. **63**, 2887 (1994).

[52] R. Radhakrishnan, A. Kundu, and M. Lakshmanan, Phys. Rev. E **60**, 3314 (1999).

[53] Y.S. Kivshar and B. Luther-Davies, Phys. Rep. **298**, 81 (1998).
[54] J.H. Marburger and E. Dawes, Phys. Rev. Lett. **21**, 556 (1968).
[55] T.K. Gustafson, P.L. Kelley, R.Y. Chiao, and R.G. Brewer, Appl. Phys. Lett. **12**, 165 (1968).
[56] W. Krolikowski and B. Luther-Davies, Opt. Lett. **18**, 188 (1993).
[57] W. Krolikowski and B. Luther-Davies, Opt. Lett. **17**, 1414 (1992).
[58] W. Krolikowski, N. Akhmediev, and B. Luther-Davies, Phys. Rev. E **48**, 3980 (1993).
[59] N. A. Kudryashov, Phys. Lett. A **427**, 127913 (2022).
[60] N. A. Kudryashov, Optik **265**, 169454 (2022).
[61] G. P. Agrawal, *Nonlinear Fiber Optics*, 4th ed. (Academic Press, 2006).
[62] K. Tai, A. Hasegawa, and A. Tomita, Phys. Rev. Lett. **56**, 135-138 (1986).
[63] T. B. Benjamen and J. E. Feir, J. Fluid. Mech. **27**, 417 (1967).
[64] C. S. Panguetna, C. B. Tabi, and T. C. Kofané, Phys. Plasmas **24**, 092114 (2017).
[65] C. B. Tabi, C. S. Panguetna, and T. C. Kofané, Physica B **5C**, 370 (2018).
[66] C. S. Panguetna, C. B. Tabi, and T. C. Kofané, Commun. Nonl. Sci. Numer. Simul. **55**, 326 (2018).
[67] K. K. Ndebele, C. B. Tabi, and T. C. Kofané, J. Op. Soc. Am. B **37**, A214 (2020) .
[68] K. K. Ndebele, C. B. Tabi, C. G. Tiofack Latchio, and T. C. Kofané, Phys. Rev. E **104**, 044208 (2021).
[69] D. Zanga, S. I Fewo, C. B. Tabi, and T. C. Kofané, Phys. Rev. A **105**, 023502 (2022).
[70] M. Abemgnigni Njifon, C. B. Tabi, and T. C. Kofané, J. Opt. Soc. Am. B **37**, A331 (2020).
[71] L. Megne Tiam, C. B. Tabi, and T. C. Kofané, Phys. Rev. E **102**, 042207 (2020).
[72] Y. S. Kivshar and M. Peyrard, Phys. Rev. A **46**, 3198 (1992).
[73] C. B. Tabi, A. D. Koko, R. O. Doko, H. P. E. Fouda, and T. C. Kofané, Physica A **442**, 498 (2016).
[74] C. B. Tabi, I. Maïna, A. Mohamadou, H. P. F. Ekobena, and T. C. Kofané, Physica A **435**, 1 (2015).
[75] C. B. Tabi, A. Mohamadou, and T. C. Kofané, J. Phys. Cond. Matter **21**, 335101 (2009).
[76] P. Otlaadisa, C. B. Tabi, and T. C. Kofané, Phys, Rev. E **103**, 052206 (2021).
[77] C. B. Tabi, S. Veni, and T. C. Kofané, Phys. Rev. A **104**, 033325 (2021).
[78] C. B. Tabi, S. Veni, and T. C. Kofané, Phys. Lett. A **442**, 128192 (2022).
[79] C. B. Tabi, P. Otlaadisa, and T. C. Kofané, Phys. Lett. A **449**, 128334 (2022).
[80] Y. S. Kivshar, D. Anderson and M. Lisak, Phys. Scr. **47**, 679 (1993).
[81] M. Soljacic, M. Segev, T. Coskun, D. N. Christodoulides, and A. Vishwanath, Phys. Rev. Lett. **84**, 467 (2000).
[82] J. F. Corney and O. Bang, Phys. Rev. Lett **87**, 133901 (2001).
[83] A. Dermican and U. Bandelow, Opt. Commun, **181**, 244 (2005).
[84] M. Peccianti, C. Conti, and G. Assanto, Phys. Rev. E **68**, 025602(R) (2003).
[85] W. Krolikowski, O. Bang, J. Rasmussen, and J. Wyller, Phys. Rev. E **64**, 16612 (2001).
[86] J. Wyller, W. Krolikowski, O. Bang, and J. Rasmussen, Phys. Rev. E **66**, 066615 (2002).
[87] P. Walczak, S. Randoux, and P. Suret, Phys. Rev. Lett. **114**, 143903 (2015).
[88] J. M. Soto-Crespo, N. Devine, and N. Akhmediev, Phys. Rev. Lett. **116**, 103901 (2016).
[89] J. M. Dudley, G. Genty, and B. J. Eggleton, Opt. Express **16**, 3644 (2008).
[90] S. Birkholz, E. T. J. Nibbering, C. Brée, S. Skupin, A. Demircan, G. Genty, and G. Steinmeyer, Phys. Rev. Lett. **111**, 243903 (2013).
[91] M. Leonetti and C. Conti, Appl. Phys. Lett. **106**, 254103 (2015).
[92] D. Pierangeli, M. Flammini, L. Zhang, G. Marcucci, A. J. Agranat, P. G. Grinevich, P. M. Santini, C. Conti, and E. DelRe, Phys. Rev. X **8**, 041017 (2018).
[93] A. Mussot, C. Naveau, M. Conforti, A. Kudlinski, F. Copie, P. Szriftgiser, and S. Trillo, Nature Photon. **12**, 303 (2018).
[94] J. M. Soto-Crespo, N. Devine, and N. Akhmediev, Phys. Rev. A **96**, 023825 (2017).
[95] C.G.L. Tiofack, S. Coulibaly, M. Taki, S. De Bièvre, and G. Dujardin, Phys. Lett. A **381**, 1999 (2017).
[96] V. V. R. K. Kumar, A. George, and P. Russel, Opt. Express **11**, 2641 (2003).
[97] L. Brilland, F. Smektala, G. Renversez, T. Chartier, J. Troles, T. N. Nguyen, N. Traynor, and A. Monteville, Opt. Express **14**, 1280 (2006).
[98] C. N. Ironside, T. J. Cullen, B. S. Bhumbra, J. Bell, W. C. Banyai, N. Finlayson, C. T. Seaton, and G. I. Stegeman, J. Opt. Soc. Am. B **5**, 492 (1988).
[99] J. L. Coutaz and M. Kull, J. Opt. Soc. Am. B **8**, 95 (1991).
[100] D. W. Hall, M. A. Newhouse, N. F. Borrelli, W. H. Dumbaugh, and D. L. Weidman, Appl. Phys. Lett. **54**, 1293 (1989).
[101] I. Kang, T. D. Krauss, F. W. Wise, B. G. Aitken, and N. F. Borrelli, J. Opt. Soc. Am. B **12**, 2053 (1995).
[102] P. Fakhri, M. R. R. Vaziri, B. Jaleh, and N. P. Shabestari, J. Opt. **18**, 015502 (2016).
[103] R. F. Souza, M. A.R.C. Alencar, M. R. Meneghetti, and J. M. Hickmann, Optical Mater. **31**, 1591 (2009)
[104] M. Segev, B. Crosignani, A. Yariv, and B. Fischer, Phys. Rev. Lett. **68**, 923 (1992).
[105] C. Conti, M. Peccianti, and G. Assanto, Phys. Rev. Lett. **91**, 73901 (2003).